Generalization of soft phonon modes

Sven P. Rudin

Generalization of Soft Phonon Modes

Sven P. Rudin

Los Alamos National Laboratory, Los Alamos, New Mexico 87545, USA and

Institute for Materials Science, Los Alamos, New Mexico 87545, USA

Abstract

Soft phonon modes describe a collective movement of atoms that transform a higher-symmetry crystal structure into a lower-symmetry crystal structure. Such structural transformations occur at finite temperatures, where the phonons (i.e., the low-temperature vibrational modes) and the static, perfect crystal structures provide an incomplete picture of the dynamics. Here, principal vibrational modes (PVMs) are introduced as descriptors of the dynamics of a material system with N atoms. The PVMs represent the independent collective movements of the atoms at a given temperature. Molecular dynamics (MD) simulations, here in the form of quantum MD (QMD) using density functional theory calculations, provide both the data describing the atomic motion and the data used to construct the PVMs. The leading mode, PVM_0, represents the $3N$-dimensional direction in which the system moves with greatest amplitude. For structural phase transitions, PVM_0 serves as a generalization of soft phonon modes. At low temperatures, PVM_0 reproduces the soft phonon mode in systems where one phonon dominates the phase transformation. In general, multiple phonon modes combine to describe a transformation, in which case PVM_0 culls these phonon modes. Moreover, while soft phonon modes arise in the higher-symmetry crystal structure, PVM_0 can be equally well calculated on either side of the structural phase transition. Two applications demonstrate these properties, first, transitions into and out of bcc titanium, and second, the two crystal structures proposed for β-phase of uranium, the higher-symmetry structure of which stabilizes with temperature.

I. INTRODUCTION

Atoms in a solid move constantly, and understanding their movement is key to understanding the solid's mechanical and thermal behavior. Descriptions of macroscopic behavior depend on judiciously merging the dynamic behavior at the atomic scale. Connecting the understanding across length scales requires culling the collective motion of the N atoms, which is a challenge because N is so large. Hence, we codify our understanding of the N atoms' varying positions by extracting meaningful descriptors. For example, in crystalline solids we refer to the average position of the atoms as the crystal structure.

Starting from the crystal structure, phonons capture the collective movement of the atoms at individual frequencies. The phonon modes describe the motion of the atoms in the harmonic approximation, which allows them to be calculated from the forces of a static crystal with the appropriate atomic displacements[1]. At low temperatures, the $3N$ phonons interact minimally, and meaningful descriptors such as the heat capacity can be evaluated using statistical mechanics[2]. A plethora of applications employing density functional theory calculations has shown this procedure to be successful at describing and predicting many properties of a vast range of materials[3–6].

In some materials, individual phonon modes stand out to signal a structural phase transformation[7]. Such a "soft phonon" in a higher-symmetry structure describes the collective motion of the atoms that take the system to a lower-symmetry structure. As the phase transition is approached the soft phonon foreshadows the coming change with a marked lowering of its frequency. The soft modes provide clear understanding of, e.g., why and how the high-temperature, body-centered cubic (bcc) Ti structure disappears as temperature is lowered: the soft modes point directly to the low-temperature hexagonal close-packed (hcp) and omega (ω-Ti) Ti structures[8].

Understanding the details of structural phase transitions in Ti and other materials leads to better control of the transitions. Many materials exhibit technologically useful phases, but in a temperature range that is not suited for specific applications. Alloying or doping with other elements can lead to a more favorable temperature range, and significant research goes into the atomistic understanding of how the added elements best affect the phase transition.

The suitability of phonons as a basis for understanding a material has limits. Materials are not static, the atoms continuously move, and with increasing temperature the phonons

interact. Eventually, at high temperatures, the phonons lose their independent nature, diminishing their usefulness as fundamental building blocks for descriptors. Phonons are low-temperature collective excitations, collective motion at high temperature needs a different description. The work presented here shows how such descriptors derive from atomistic simulations of materials.

Quantum molecular dynamics (QMD) accurately represent the atomic motion, and from it collective behavior can be extracted. With the data from QMD simulations correlations can be quantified, and new displacement patterns can be built based on the correlations. With this approach, the QMD data serves two purposes: it provides both the "raw" information of how the atoms interact and the framework in which to look at the information.

Section II outlines the formalism employed here to extract and put to use correlations from QMD simulations. Rotating the $3N$-dimensional basis of the displacements to reflect the correlations results in a new set of modes that are no longer correlated with each other: each of the new modes describes an independent collective movement of the atoms that reflects some principle activity in the material. Here such a mode is referred to as a Principle Vibrational Mode (PVM). Section III demonstrates applications of the formalism, first to the structural transformations into and out of the body-centered cubic (bcc) Ti structure, and second to two proposed structures for the β-phase of uranium.

II. METHOD

Experimental scattering methods provide information about atomic motion in condensed matter. The measured spectrum is represented by the dynamic structure factor $S(\mathbf{Q}, \omega)$[9], first introduced by van Hove[10,11]. $S(\mathbf{Q}, \omega)$ relates to the atomic positions by way of temporal and spatial Fourier transforms: the spatial Fourier transformation of the time-dependent positions $\mathbf{r}_i(t)$ of the N atoms defines a wave vector $\mathbf{Q}$-dependent particle density operator,

$$\rho(\mathbf{Q}, t) = \sum_{i=1}^{N} e^{-i\mathbf{Q} \cdot \mathbf{r}_i(t)}. \tag{1}$$

The temporal Fourier transformation,

$$S(\mathbf{Q}, \omega) = \int_{-\infty}^{\infty} e^{-i\omega \cdot t} F(\mathbf{Q}, t) dt, \tag{2}$$

transforms the correlation of the particle density, known as the intermediate scattering function and given by

$$F(\mathbf{Q}, t) = \frac{1}{N} \langle \rho(\mathbf{Q}, t)\rho(-\mathbf{Q}, 0) \rangle. \tag{3}$$

This formalism serves equally well to extract theoretical spectra from QMD simulations[12].

The work presented here employs a formalism that modifies the above to extract descriptors of the collective atomic motion in a QMD simulation. First, the time-dependent positions $\mathbf{r}_i(t)$ of the N atoms are tracked in terms of the displacement of the atoms from a crystal structure's sites $\mathbf{R}_i$, $\delta\mathbf{r}_i(t) = \mathbf{r}_i(t) - \mathbf{R}_i$. Second, the particle density operators are described in a basis $\{\mathbf{B}_n\}$ that reflects the correlations extracted from the QMD simulation,

$$\rho_{\mathbf{B}_n}(t) = \sum_{i=1}^{N} \mathbf{B}_n \cdot \delta\mathbf{r}_i(t). \tag{4}$$

Finding the basis $\{\mathbf{B}_n\}$ relies on analyzing the QMD data.

This analysis of the QMD data is performed in terms of an orthonormal set of $3N$ basis vectors for the atomic displacements with respect to a crystal structure, $\{\mathbf{e}_j\}$. These basis vectors are not the basis $\{\mathbf{B}_n\}$, but a necessary step in finding the basis $\{\mathbf{B}_n\}$. Here the eigenvectors of the phonon modes serve as the $\{\mathbf{e}_j\}$, calculated using density functional perturbation theory. These basis vectors define the instantaneous amplitude of the phonon modes,

$$\tilde{\rho}(\mathbf{e}_j, t) = \sum_{i=1}^{N} \mathbf{e}_j \cdot \delta\mathbf{r}_i(t), \tag{5}$$

and the time-dependent correlation of each phonon mode,

$$\tilde{F}(\mathbf{e}_j, t) = \frac{1}{N} \langle \tilde{\rho}(\mathbf{e}_j, t)\tilde{\rho}(\mathbf{e}_j^*, 0) \rangle. \tag{6}$$

An advantage of using the eigenvectors of the phonon modes as the $\{\mathbf{e}_j\}$ arises for the analysis applied to a system with multiple elements: the eigenvectors of the phonon modes scale the atomic displacements according to the different masses of the elements.

The correlations between phonon modes are codified in the matrix

$$\underline{C}_{\mathbf{e}_j, \mathbf{e}_k} = \int_{-\infty}^{\infty} \tilde{F}(\mathbf{e}_j, t)\tilde{F}(\mathbf{e}_k, t)dt. \tag{7}$$

This definition of correlations between phonon modes is not unique but well suited for the current application to structural phase transformations. Principle component analysis of $\underline{C}$

4

leads to the basis in which the descriptors of the atomic motion are decorrelated; specifically, diagonalization provides the eigenvectors $\mathbf{v}_n$ of $\underline{C}$ which define $\{\mathbf{B}_n\}$,

$$\mathbf{B}_n = \sum_j \mathbf{v}_n(j) \cdot \mathbf{e}_j. \tag{8}$$

Inserting the particle density operator of Eq. 4 into Eqs. 2 and 3 produces the spectra for PVM_n.

By construction, the eigenvector $\mathbf{v}_0$ with the largest eigenvalue defines the mode with the largest root mean squared amplitude. This mode, referred to here as the leading principle vibrational mode, PVM_0, represents the direction in the $3N$-dimensional space in which one collective motion of atoms probes the deepest. This and succeeding modes with large amplitudes in a material are often critical properties for the material's application, and the leading PVMs can serve as theoretical descriptors. Across a structural phase transformation, the movement of atoms needed to describe the transformation involves a large, finite displacement and is hence reflected in PVM_0 as shown in Section III.

Application of the formalism involves choosing a reference crystal structure, which defines the crystal structure sites $\mathbf{R}_i$. Across structural phase transformations, both connected crystal structures serve as reference structures in two independent analyses. Taken together, they provide complementary insight into the atomic motion described by the QMD data.

The QMD data analyzed here originate in density functional theory calculations using the VASP package[13,14]. The QMD calculations simulate a fixed number of atoms in a fixed simulation cell with constant energy. For comparison with experiment, QMD simulations with fixed pressure rather than fixed simulation cell would be preferable, but the resulting changes to cell dimensions and shape remain outside the current implementation of the formalism. Similarly, fixed temperature would be preferable over fixed energy, and indeed using a Nosé thermostat (with Nosé mass corresponding to a frequency 5 THz) delivers results in general agreement with those presented here. Sections III A and III B discuss the chosen simulation cell shapes. The constant energy values are set by preparatory QMD calculations that scale the velocities to set sequences of temperatures for each system. The electrons are treated in the generalized gradient approximation of Perdew, Burke, and Ernzerhof[15]. No additional specific treatment of the spin-orbit coupling or f-electron correlation effects in uranium are included[16]. The electronic energy, treated in the PAW method[17], is evaluated at each atomic time step of 5 fs with Methfessel–Paxton smearing, $\sigma = 0.1$ eV, and Fermi-
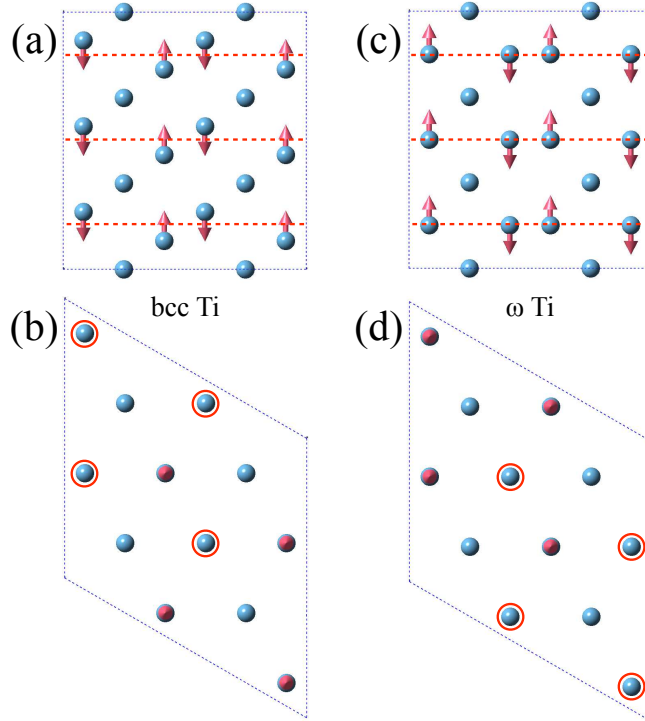
FIG. 1. (Color online) Schematic of the structural phase transformation between bcc-Ti and ω-Ti. A $2 \times 2 \times 3$ supercell is shown from the side (a, c) and from the top (b, d) for the two crystal structures, respectively. Arrows indicate the directions and relative magnitudes of the atoms' pathways that transform the solid from one crystal structure to the other. The dashed, red line represents the hexagonal plane present in ω-Ti.

Dirac smearing, $\sigma = 0.027$ eV, for Ti and U, respectively, with a convergence criteria of 10^{-5} eV. The k-point meshes rely on $2 \times 2 \times 2$ and $6 \times 6 \times 6$ grids for Ti and U, respectively.

III. RESULTS

A. Ti bcc to ω Transition

Structural transformations in Ti receive a lot of attention[18]. On the technological side, Ti plays a major role in industrial applications requiring light weight, high strength, and corrosion resistance. On the scientific side, the high-temperature bcc phase of Ti exhibits soft phonon modes directly linked to low-temperature phases[8]. DFT calculations of the bcc Ti phonons show these modes as unstable at zero temperature[19]. Because of these instabilities, Ti is frequently invoked as a test system for methods aimed at calculating

vibrational properties of mechanically unstable high-temperature phases[20,21].

The titanium QMD calculations employ simulation cells chosen to represent both bcc and ω crystal structures. The calculations are performed at a volume of 18.13 Å^3/atom in a hexagonal unit cell with $c/a = 0.612$. The simulation cells encompass $2 \times 2 \times 3$, $3 \times 3 \times 4$, or $4 \times 4 \times 6$ unit cells containing three atoms each. With Ti atoms placed at $(0,0,0)$, $(\frac{1}{3}, \frac{1}{3}, \frac{1}{3})$, and $(\frac{2}{3}, \frac{2}{3}, \frac{2}{3})$, the unit cells describe a bcc lattice with a lattice constant of 3.31 Å[22]. Placing the Ti atoms at $(0,0,0)$, $(\frac{1}{3}, \frac{1}{3}, \frac{1}{2})$, and $(\frac{2}{3}, \frac{2}{3}, \frac{1}{2})$ represents the ω-Ti lattice at a slightly negative pressure[23]. Figure 1 illustrates the two structures and the atoms' pathways connecting them in the $2 \times 2 \times 3$ supercell.

The two larger systems in the QMD simulations undergo the expected structural transformations. In the current computational framework, the low-temperature ω-Ti structure transforms into the bcc structure when the average temperature increases above around 800 K ($3 \times 3 \times 4$ supercell) or around 600 K ($4 \times 4 \times 6$ supercell). Conversely, decreasing the average temperature below around 800 K ($3 \times 3 \times 4$ supercell) or around 600 K ($4 \times 4 \times 6$ supercell) transforms the high-temperature bcc structure into a hcp structure with line defects. The hcp structure is expected at this volume, but the simulation cell does not allow a complete transformation into perfect hcp.

The $2 \times 2 \times 3$ simulation cell retains the ω-Ti structure up to average temperatures around 800 K. For average temperatures above around 900 K, the system transforms but fails to stabilize a flawless bcc structure. The number of phonons commensurate with the small supercell is insufficient to support the phonon-phonon interactions needed to stabilize the bcc crystal structure. Hence, the remainder of this work focuses on the two larger systems.

Figure 2 shows the resulting PVM$_0$ for ω-Ti at low temperature ($3 \times 3 \times 4$ supercell). Evaluated in the bcc basis, PVM$_0$ exhibits near-static behavior (its spectrum peaks sharply at zero frequency) and describes the atomic displacements needed to take bcc into the ω-Ti structure. These displacements, projected into the phonon mode basis $\mathbf{e}_j$, are those of one unstable phonon mode, corresponding to the displacements shown in Fig. 1. Five independent simulations, with average temperatures between 44 K and 51 K, all have PVM$_0$ described by the same unstable phonon mode. Analyzed in the ω-Ti basis, the PVM$_0$ of the five independent simulations are all dominated by linear combinations of the degenerate phonon modes with frequency 2.6 THz, with weight between 0.93 and 0.96. The remaining phonon modes contributing to PVM$_0$ differ between the the simulations, but come from
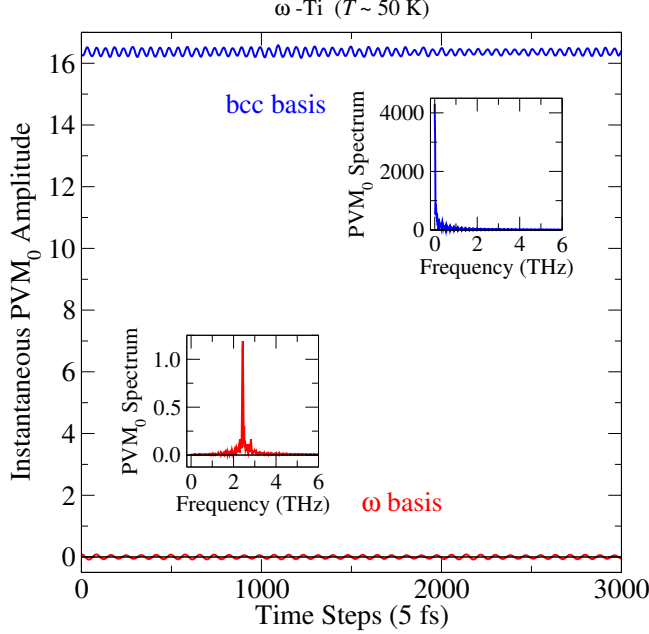
FIG. 2. (Color online) PVM_0 for ω-Ti ($3\times3\times4$ supercell) at 50 K evaluated in the ω basis (red) and in the bcc basis (blue). The system on average assumes the ω-Ti structure, and the instantaneous amplitude of PVM_0 averages to zero in the ω basis; the spectrum of PVM_0 shows a sharp peak at 2.4 THz. In the bcc basis, the system has transformed away from the bcc-Ti structure, hence PVM_0 acquires a nearly constant, finite amplitude; consequently the spectrum of PVM_0 is sharply peaked at zero. The offset of the instantaneous PVM_0 amplitude evaluated in the bcc basis reflects the sum of all atomic displacements that connect the atomic positions in the bcc structure with the average atomic positions in the simulation.

phonon modes with similar frequencies (between 2.0 and 2.8 THz). PVM_0 in the ω-Ti basis exhibits near-harmonic behavior with a sharply peaked spectrum at 2.4 THz for the $3 \times 3 \times 4$ supercell and at 2.0 THz for the $4 \times 4 \times 6$ supercell. This lowering of frequency is consistent with PVM_0 representing the direction in $3N$-dimensional space in which one collective motion of atoms probes the deepest: as the simulation cell is increased, longer wave length phonon modes become commensurate with the cell, and they generally have lower frequencies.

At high temperatures, Ti adopts the bcc crystal structure. Compared to low temperatures, this reverses the roles of the ω-Ti and bcc structures in the PVM analysis. This reversal of roles appears in Fig. 3 ($3 \times 3 \times 4$ supercell). The amplitude of PVM_0 now ex-
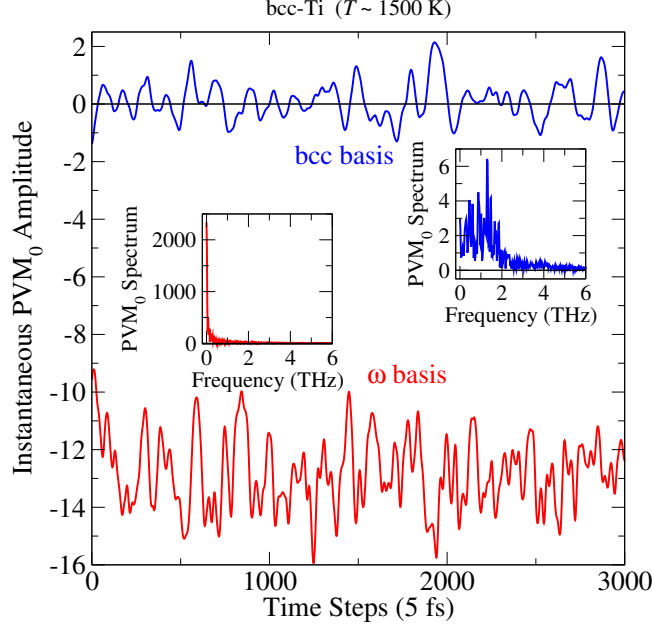
FIG. 3. (Color online) PVM_0 for bcc-Ti ($3 \times 3 \times 4$ supercell) at 1500 K evaluated in the bcc basis (blue) and in the ω basis (red). The system on average acquires the bcc-Ti structure, and PVM_0 exhibits strongly non-harmonic behavior that averages to zero in the bcc basis; the spectrum of PVM_0 shows a peak at 1.3 THz, but other low frequencies are present. In the ω basis, the system has transformed away from the ω-Ti structure, and the average of PVM_0 assumes a finite amplitude; the spectrum of PVM_0 is sharply peaked at zero.

hibits a finite average value in the ω basis, albeit with larger fluctuations due to the higher temperature. The atomic displacement superimposes the displacement patterns defined by mainly the phonon modes with frequencies 4.2 and 6.1 THz, which have polarizations mainly in the direction of the transformation (see Fig. 1(c)). Evaluated in the bcc basis, the instantaneous amplitude of PVM_0 exhibits large fluctuations centered around zero. At this temperature, the system contains significant anharmonicity, as evident from the spectrum of PVM_0 – and the fact that the bcc crystal structure appears stable.

Table I lists the main phonon modes whose displacement patterns contribute to the PVM_0 for bcc-Ti in five QMD simulations with average temperatures near 1500 K. The atomic motion described by PVM_0 is described dominantly by phonon modes that are unstable at zero temperature. Which phonon mode dominates varies between simulations.

The formalism performs equally well in a QMD simulation that includes a structural phase transformation. Figure 4 shows an example in which the $3 \times 3 \times 4$ supercell system

9

| phonon frequencies (THz): | | | | 1.56 | −0.41 | −0.62 | −2.18 | −2.91 | −3.28 | −3.68 | −4.32 | −5.00 |
| $\langle T \rangle$ | f_{max} | f_{fit} | σ | | | | phonon mode weights in PVM_0 | | | | | |
(K)		(THz)										
run 1	1460	1.76	1.37	0.71	0.01	0.00	0.03	0.07	0.83	0.00	0.02	0.02	0.01
run 2	1473	1.30	1.01	0.73	0.00	0.01	0.92	0.00	0.01	0.02	0.00	0.02	0.00
run 3	1483	1.30	1.25	0.77	0.09	0.00	0.57	0.02	0.03	0.00	0.26	0.01	0.01
run 4	1517	1.62	1.32	0.44	0.06	0.00	0.75	0.07	0.09	0.00	0.01	0.00	0.00
run 5	1530	1.56	1.38	0.60	0.01	0.00	0.01	0.51	0.41	0.01	0.00	0.02	0.01

TABLE I. Frequencies describing PVM_0 for bcc-Ti in QMD simulations with average temperatures around 1500 K ($3 \times 3 \times 4$ supercell). The five simulations are ordered by their average temperature, $\langle T \rangle$. The peak in the spectrum of each simulation's PVM_0, f_{max}, is reported along with a fit of the spectrum to a Gaussian centered at f_{fit} with variance σ. The phonon modes listed are those that contribute to the PVM_0 of at least one simulation with a weight of at least 0.01, where the reported weight sums contributions from all degenerate modes.
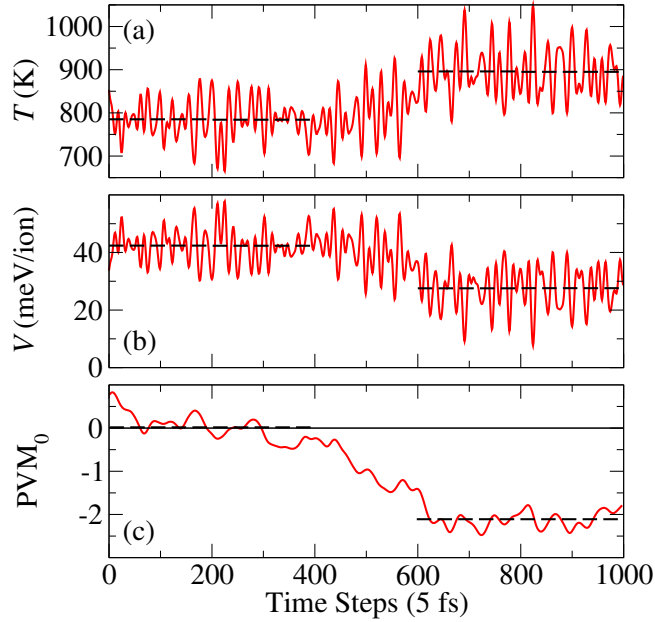
FIG. 4. (Color online) Temperature, potential energy, and instantaneous amplitude of PVM_0 for Ti in a QMD simulation showing the structural transformation from bcc to hcp with line defects ($3 \times 3 \times 4$ supercell). Data extracted from the QMD simulation is shown in red; black dashed lines are the averages for the first and last 200 time steps, respectively.

goes from the bcc crystal structure to the hcp structure containing line defects. Because the hcp structure lies lower on the potential energy surface, the potential energy moves from a higher to a lower average, while the kinetic energy, and hence the temperature, increase from a lower to a higher average. Evaluated in the bcc basis (applying the formalism to the full sequence of steps in Fig. 4), PVM_0 culls contributions from the displacement patterns of many phonon modes, the majority of which are unstable at zero temperature. The PVM_0 starts with fluctuations around zero while in the bcc structure, and then moves to values that fluctuate around a finite value once the transformation concludes. The same behavior appears in the $4 \times 4 \times 6$ supercell, though the details differ: for example, the transformation starts and ends with lower average temperatures, around 650 K and 780 K, respectively, because the increased number of modes commensurate with the larger cell allows for better resolution of in particular low-frequency modes, whose entropy contribution lowers the free energy of the bcc phase.

Figure 5 maps the atomic displacement pattern of PVM_0 onto the atomic displacement patterns of the phonon modes of the bcc structure ($3 \times 3 \times 4$ supercell). The figure plots the weights of the phonon modes in PVM_0 on a logarithmic scale because the dominant contributing phonon mode generally has a much larger weight than the other phonon modes. In the bcc Ti structure, simulated at $\langle T \rangle \approx 880$ K, unstable zero-temperature phonon modes dominate PVM_0. At this temperature, strong anharmonicity introduces correlation between the atomic motions of these modes, causing them to appear stable in both measurements (with finite lifetime)[8] and calculations[20].

The mapping in Fig. 5 corresponds to the simulation in Fig. 4 and one simulation each with average temperature 700 K and 880 K, respectively. Independent QMD simulations ($3 \times 3 \times 4$ supercell) with average temperatures close to those of the shown simulations agree with the results reported in the previous paragraphs. Differences arise in which of the phonon modes represent the atomic motion of the PVM_0, but in all cases, those modes that contribute with a weight larger than 0.01 are unstable phonon modes. Differences also appear in how long the structures remain stable: the hcp structure with line defects generally remains stable throughout the simulations (up to 25 ps), while the bcc structure simulated around 780 K transforms after at most 5 ps and rarely exceeds 15 ps for average temperatures around 880 K.

As mentioned in Sec. II, PVM_0 represents the direction in the $3N$-dimensional space
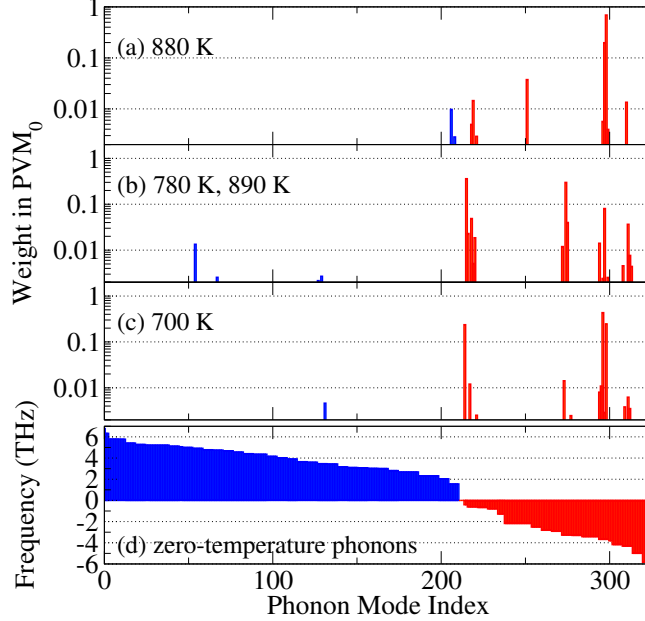
FIG. 5. (Color online) Weights of the phonon modes in the PVM_0 of Ti ($3 \times 3 \times 4$ supercell) referenced to the bcc structure (a-c), and frequencies of the (zero-temperature) phonon modes (d). The weights are obtained by projecting the atomic displacements in PVM_0 onto the displacement patterns defined by the phonon modes. The phonon modes (d) are indexed from highest to lowest frequency for the stable modes (blue), followed by the unstable modes (red) from lowest to highest imaginary frequency (plotted as negative frequencies). The color code is retained in (a-c) as a visual aid. At 880 K the average atomic positions are on the bcc lattice, at 700 K they are on the hcp lattice with line defects. Subplot (b) shows the weights for the QMD simulation shown in Fig. 4, where the system transforms from bcc to hcp with line defects.

with the largest amplitude. Figure 5 shows that across the structural phase transition in Ti unstable phonon modes of the bcc structure contribute significantly to PVM_0. These are the known instabilities of the bcc structure that take it to the lower-symmetry and lower-temperature structures. However, the phonon modes with relevant contributions to PVM_0 of bcc Ti also remain relevant in the low-temperature structure. This connection indicates that the directions with the largest amplitude for these high- and low-temperature phases of Ti are intimately linked. As shown below, such a link does not connect the two structures analyzed for the β phase of U.
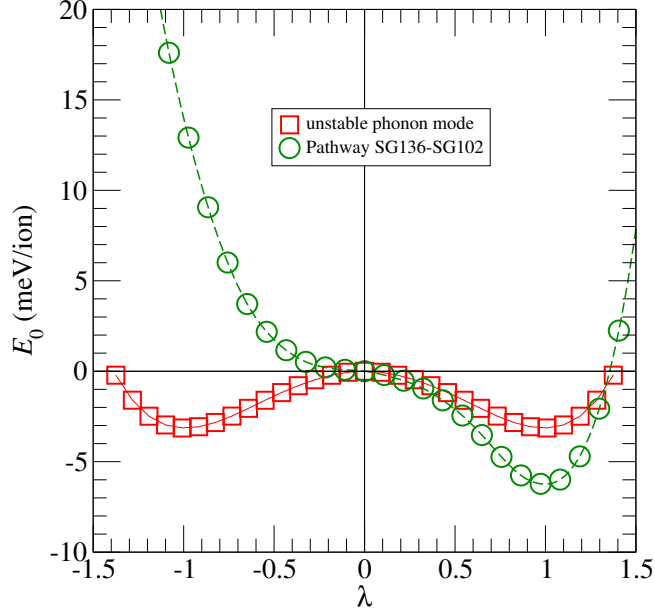
FIG. 6. (Color online) Calculated projections of the energy landscape around the space group 136 ($\lambda = 0$) structure of β-U. Displacing the atoms according to the pattern described by the unstable phonon mode (red) lowers the energy in either direction (with $\lambda = 1$ defined as the amplitude that minimizes the energy). Displacing the atoms according to the pattern described by the differences in their positions in the space group 136 ($\lambda = 0$) structure and the space group 102 ($\lambda = 1$) structure lowers the energy only in the positive direction. Reversing the atomic displacements raises the energy, and this asymmetry indicates that the path connecting the two structures is defined by more than a single phonon mode.

B. β-U Crystal Structure

The β-U phase appears in a small temperature range around 1000 K, making experimental determination of the crystal structure difficult. The structure has 30 atoms in a tetragonal unit cell, but disagreement persists in the literature on the exact symmetry. Neutron powder diffraction data points to a structure with higher symmetry, space group No. 136[24], which more recent symmetry arguments support[25]. Density functional theory calculations show that a structure with lower symmetry, space group No. 102 has a lower energy[26]. The calculations furthermore show an unstable phonon mode for the higher-symmetry structure, which can lead the structure toward the lower-symmetry structure.

Figure 6 plots the energy calculated along two paths described by atomic displacement
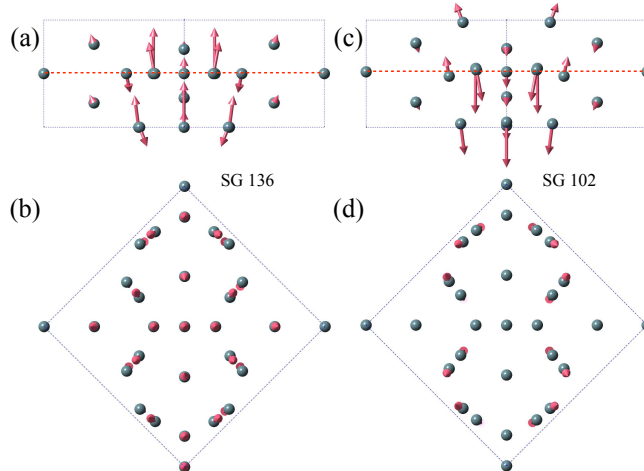
FIG. 7. (Color online) Schematic of the atomic pathways connecting the space group No. 136 and space group No. 102 crystal structures of β-U. The primitive cell is shown from the side (a, c) and from the top (b, d) for the two space groups, respectively. Arrows indicate the directions and relative magnitudes of the atoms' pathways that take the crystal structure to the other space group. The dashed, red line represents the mirror plane present in space group No. 136 but absent in space group No. 102.

from the higher symmetry structure. The path defined by the unstable phonon mode lowers the energy and is symmetric around the undistorted crystal structure. The path defined by the differences in atomic positions between the two structures, illustrated in Fig. 7, lowers the energy by roughly double the amount and is not symmetric. The calculated energy difference between the two structures is almost an order of magnitude smaller than the energy scale of the temperature at which β-U appears; this suggests a strongly anharmonic system in which the phonons interact to stabilize the higher symmetry structure. The difference in how much the two paths in Fig. 6 lower the energy, as well as the asymmetry in the energy of the path defined by the structural differences, suggest multiple phonon modes combine to describe the path. These points motivate performing QMD simulations on these structures and applying the PVM analysis.

The β-U QMD calculations employ fixed simulation cells that can represent both proposed crystal structures. The simulation cells are made close to cubic by doubling the unit cells, which were optimized for both structures independently. The QMD simulations employ a k-point mesh of $6 \times 6 \times 6$. The total energies agree with those of a k-point mesh of $8 \times 8 \times 8$
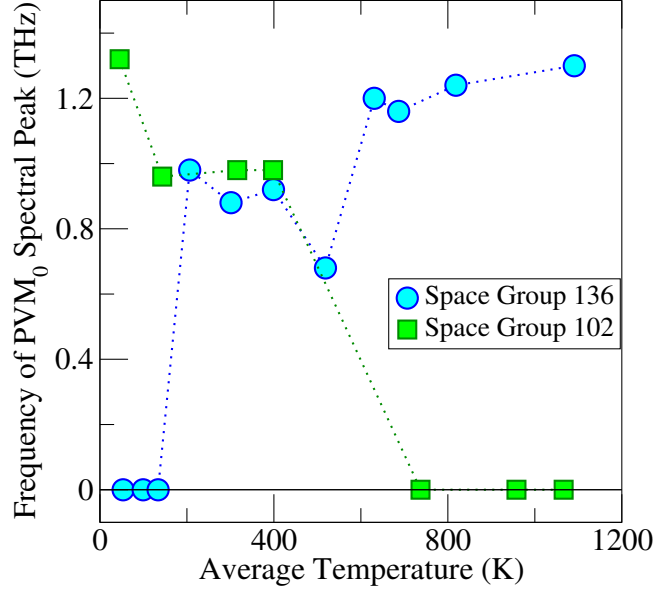
FIG. 8. (Color online) Frequencies of the spectral peak for the PVM_0 of β-U at different average temperatures of the QMD simulations. Dashed lines are to guide the eye. The spectral peaks for the PVM_0 of the lower-symmetry structure (space group No. 102) remain finite up to $\langle T \rangle \approx 400$ K, while the spectral peaks for the PVM_0 of the higher-symmetry structure (space group No. 136) remain finite down to $\langle T \rangle \approx 200$ K.

to within $2 \cdot 10^{-5}$ eV. In a comparison of the phonons calculated with the two mesh densities, the stable modes' phonon frequencies agree to within at worst 2%, and the unstable mode's imaginary frequency differs by 0.2%. A less dense mesh appears insufficient: the total energy agrees to within 0.2 meV/atom for a k-point mesh of $4 \times 4 \times 4$, but the agreement for the phonons is significantly worse, hence the QMD simulations employ the $6 \times 6 \times 6$ k-point mesh.

Figure 8 shows the stability of the higher-symmetry structure in a range of temperatures above and well below 1000 K. The lower-symmetry structure, on the other hand, becomes unstable for high temperatures. At lower temperatures, the structure with lower symmetry appears metastable in these QMD simulations, but the stable α-U structure preclude experimental observation of it.

In the higher-symmetry structure, Figure 8 shows the frequency of the PVM_0 spectral peak varying non-monotonically before the transformation. This variation, however, should not be attributed to a particular phonon mode: the spectra of PVM_0 at different tempera-
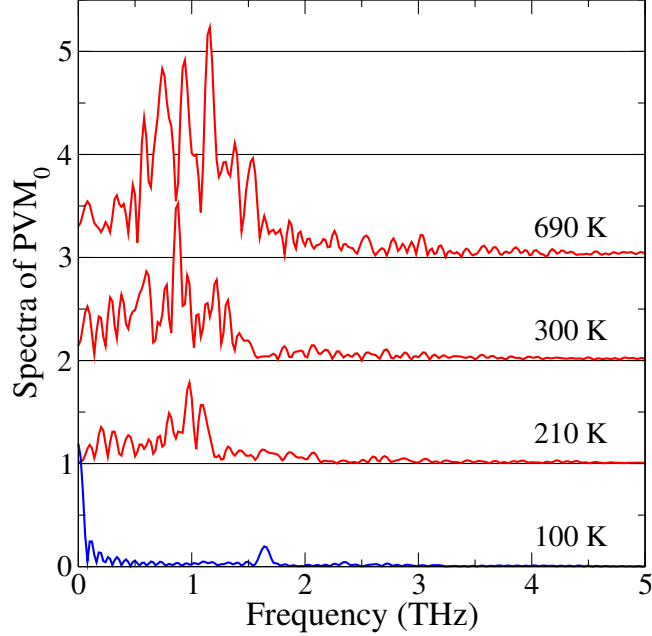
FIG. 9. (Color online) Spectra for the PVM_0 of β-U, references to the higher-symmetry structure (space group No. 136), at average temperatures of the QMD simulations above (red) and below (blue) the transition. Above $\langle T \rangle \approx 200$ K, the spectra for the PVM_0 reveal contributions from many low frequencies. At 100 K, the system has transformed into the lower-symmetry structure, and the spectrum becomes dominated by the peak at 0 THz.

tures in Fig. 9 show that the variation reflects a change in which vibrational modes dominate the atomic motion.

Figure 10 provides the same insight by mapping the atomic displacement pattern of PVM_0 onto the atomic displacement patterns of the phonon modes. At 690 K, the dominant contribution is from a stable zero-temperature phonon mode with harmonic frequency 1.48 THz. At 300 K and 210 K, the dominant contribution is from a phonon mode with harmonic frequency 0.80 THz. Strong anharmonicity introduces correlation between the atomic motions of these dominant phonon modes and other (stable and unstable) phonon modes. While the latter contribute to the atomic displacement pattern of PVM_0 with much less weight (Fig. 10), they strongly affect the spectrum of PVM_0 (Fig. 9).

Below the transition temperature, the atomic displacement pattern of PVM_0 combines the atomic displacement patterns of mainly stable zero-temperature phonon modes. The dominant contribution (49%) is from the phonon mode with harmonic frequency 2.48 THz, followed by the phonon mode with harmonic frequency 1.48 THz (30%). This latter mode

16
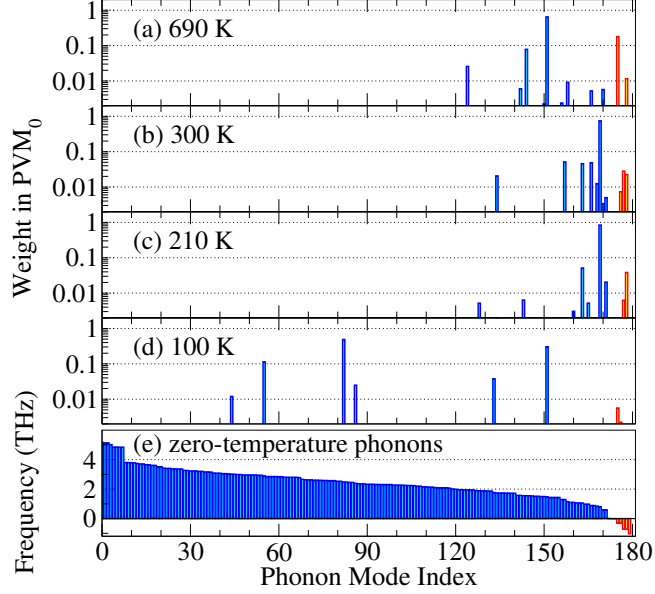
FIG. 10. (Color online) Weights of the (zero-temperature) phonon modes in the PVM_0 of β-U (a-d), references to the higher-symmetry structure (space group No. 136), at average temperatures of the QMD simulations above (690 K, 300 K, 210 K) and below (100 K) the transition, and frequencies of the (zero-temperature) phonon modes (e). The weights are obtained by projecting the atomic displacements in PVM_0 onto the displacement patterns defined by the phonon modes. The phonon modes are indexed from highest to lowest frequency for the stable modes (blue), followed by the unstable modes (red) from lowest to highest imaginary frequency (plotted as negative frequencies). The color code is retained in throughout the finite-temperature results as a visual aid.

is the dominant mode for the PVM_0 at 690 K, but in general phonon modes contributing to PVM_0 above the transition temperature do not contribute significantly to PVM_0 below the transition temperature. This is in stark contrast to the structural phase transition in Ti, where many of the same phonon modes contribute to PVM_0 above and below the transition temperature (Fig. 5).

Also remarkably different from the structural phase transition in Ti, the atomic displacement pattern of PVM_0 for β-U below the transition temperature has a almost negligible contribution from unstable zero-temperature phonon modes. This stems from the small atomic displacements that take the higher-symmetry structure into the lower-symmetry structure: both the average 0.15 Å and the maximum 0.29 Å are significantly smaller than the corresponding values for the structural phase transition in Ti, 0.32 Å and 0.48 Å. The

17

fluctuations in the instantaneous PVM_0 amplitude for β-U are consequently comparable to the average PVM_0 amplitude, while for Ti the fluctuations are significantly smaller than the average.

IV. CONCLUSION

The work presented here uses data from QMD simulations as both the source of information and as the determining factor in how the information serves to advance understanding. Correlations present in the data serve to define the principle vibrational modes (PVMs) with which the data is analyzed. The atomic motion in a material simulation, expressed originally in the phonon modes, exhibits correlations between the modes. The construction of the PVMs leads to no correlation between modes.

The leading PVM, PVM_0, emerges as a descriptor of the collective motion with the largest amplitude. Because the extraction of PVM_0 does not rely on any symmetries, it can guide the study of effects of symmetry-breaking changes, e.g., doping or alloying, on technologically desired or undesired properties directly related to the direction in the $3N$-dimensional space in which one collective motion of atoms probes the deepest. While the examples in the work presented here consider systems with single elements, experience shows that the PVM analysis works equally well for compounds and alloys (to be published elsewhere).

Applied to materials with structural phase transitions, PVM_0 serves as a generalization of the soft phonon modes. It describes the complete structural transformation to the new phase in a single mode, and it can be mapped out from the crystal structure present on either side of the transformation.

Two materials show how the analysis works in practice. Across the structural transformations into and out of the body-centered cubic (bcc) Ti structure, PVM_0 describes the atomic motion needed to transform between structures. The analysis furthermore reveals a close link between the directions with the largest amplitude for the high- and low-temperature phases of Ti. In the second material, uranium, the literature disagrees on which of two structures is the correct structure for the β phase observed around 1000 K. The QMD simulations show that temperature stabilizes the high-symmetry structure, and the amplitude of PVM_0 assumes a finite or zero average when analyzed in reference to the lower-symmetry or higher-symmetry structure, respectively. For the β phase of U, the analysis reveals no

close link between the two crystal structures in terms of the $3N$-dimensional directions in which the systems move with greatest amplitude.

Both materials exhibit a structural transformation that can be attributed to phonon mode that are unstable at zero temperature. The PVM analysis reveals the presence of the atomic displacement patterns of these phonon modes in the atomic displacement patterns of PVM_0 in simulations above the transition temperature. The phonon modes that contribute the most to PVM_0 in the high-temperature phase remain important in the low-temperature phase of Ti, but not in U.

V.   ACKNOWLEDGEMENTS

[1] K. Kunc and R. M. Martin, Phys. Rev. Lett. **48**, 406 (1982).

[2] R. K. Pathria, *Statistical Mechanics* (Pergamon Press, Oxford, 1972).

[3] S. Baroni, P. Giannozzi, and E. Isaev, Rev. Miner. Geochem. **71**, 39 (2011).

[4] A. Jain, G. Hautier, C. J. Moore, S. P. Ong, C. C. Fischer, T. Mueller, K. A. Persson, and G. Ceder, Computational Materials Science **50**, 2295 (2011).

[5] A. Jain, S. P. Ong, G. Hautier, W. Chen, W. D. Richards, S. Dacek, S. Cholia, D. Gunter, D. Skinner, G. Ceder, and K. A. Persson, APL Materials **1**, 011002 (2013), https://doi.org/10.1063/1.4812323.

[6] M. de Jong, W. Chen, T. Angsten, A. Jain, R. Notestine, A. Gamst, M. Sluiter, C. Krishna Ande, S. van der Zwaag, J. J. Plata, C. Toher, S. Curtarolo, G. Ceder, K. A. Persson, and M. Asta, Scientific Data **2**, 150009 EP (2015).

[7] W. Cochran, Advances in Physics **10**, 401 (1961), https://doi.org/10.1080/00018736100101321.

[8] W. Petry, A. Heiming, J. Trampenau, M. Alba, C. Herzig, H. R. Schober, and G. Vogl, Phys. Rev. B **43**, 10933 (1991).

[9] J. P. Hansen and M. L. Klein, Phys. Rev. B **13**, 878 (1976).

[10] L. van Hove, Phys. Rev. **95**, 249 (1954).

[11] D. A. McQuarrie, *Statistical Mechanics* (Harper & Row, New York, 1976) p. 544.

[12] T. Sjostrom, S. Crockett, and S. Rudin, Phys. Rev. B **94**, 144101 (2016).

[13] G. Kresse and J. Furthmuller, Phys. Rev. B **54**, 11169 (1996).

[14] G. Kresse and D. Joubert, Phys. Rev. B **59**, 1758 (1999).

[15] J. P. Perdew, K. Burke, and M. Ernzerhof, Phys. Rev. Lett. **77**, 3865 (1996).

[16] P. Söderlind, Phys. Rev. B **66**, 085113 (2002).

[17] P. E. Blöchl, Phys. Rev. B **50**, 17953 (1994).

[18] D. Banerjee and J. Williams, Acta Materialia **61**, 844 (2013), the Diamond Jubilee Issue.

[19] K. Persson, M. Ekman, and V. Ozolins, Phys. Rev. B **61**, 11221 (2000).

[20] P. Souvatzis, O. Eriksson, M. I. Katsnelson, and S. P. Rudin, Phys. Rev. Lett **100**, 095901 (2008).

[21] N. Antolin, O. D. Restrepo, and W. Windl, Phys. Rev. B **86**, 054119 (2012).

[22] J. Spreadborough and J. W. Christian, Proceedings of the Physical Society **74**, 609 (1959).

[23] A. Dewaele, V. Stutzmann, J. Bouchet, F. m. c. Bottin, F. Occelli, and M. Mezouar, Phys. Rev. B **91**, 134108 (2015).

[24] A. C. Lawson, C. E. Olsen, J. W. Richardson, M. H. Mueller, and G. H. Lander, Acta Crystallographica Section B **44**, 89 (1988).

[25] J. Li, Q. Ren, C. Lu, L. Lu, Y. Dai, and B. Liu, Journal of Alloys and Compounds **516**, 139 (2012).

[26] Y.-R. Gong, T. Gao, G.-A. Sun, B.-Q. Liu, and B. Chen, Journal of the Korean Physical Society **66**, 234 (2015).